

Radiative rotational lifetimes and state-resolved relative detachment cross sections from photodetachment thermometry of molecular anions in a cryogenic storage ring

C. Meyer,^{1,*} A. Becker,¹ K. Blaum,¹ C. Breitenfeldt,^{1,2} S. George,¹ J. Göck,¹ M. Grieser,¹ F. Grussie,¹ E. A. Guerin,¹ R. von Hahn,¹ P. Herwig,¹ C. Krantz,¹ H. Kreckel,¹ J. Lion,¹ S. Lohmann,¹ P. M. Mishra,¹ O. Novotný,¹ A. P. O'Connor,¹ R. Repnow,¹ S. Saurabh,¹ D. Schwalm,^{1,3,†} L. Schweikhard,² K. Spruck,^{1,4} S. Sunil Kumar,¹ S. Vogel,¹ and A. Wolf¹

¹*Max-Planck-Institut für Kernphysik, D-69117 Heidelberg, Germany*

²*Institut für Physik, Ernst-Moritz-Arndt-Universität Greifswald, D-17487 Greifswald, Germany*

³*Weizmann Institute of Science, Rehovot 76100, Israel*

⁴*Institut für Atom- und Molekülphysik, Justus-Liebig-Universität Gießen, D-35392 Gießen, Germany*

(Dated: November 8, 2018)

Photodetachment thermometry on a beam of OH^- in a cryogenic storage ring cooled to below 10 K is carried out using two-dimensional, frequency and time dependent photodetachment spectroscopy over 20 minutes of ion storage. In equilibrium with the low-level blackbody field, we find an effective radiative temperature near 15 K with about 90% of all ions in the rotational ground state. We measure the $J = 1$ natural lifetime (about 193 s) and determine the OH^- rotational transition dipole moment with 1.5% uncertainty. We also measure rotationally dependent relative near-threshold photodetachment cross sections for photodetachment thermometry.

Small molecular ions and their interactions in the lowest rotational states are crucial for the formation of molecules in interstellar space and for low-temperature plasma chemistry in general [1, 2]. Both cations and anions [3] were observed in space based on rotational spectroscopy. While line positions are well studied in the laboratory for many relevant ions, experimental information on their line intensities is scarce. Instead, line strengths for ionic rotational transitions are generally obtained from calculated molecular dipole moments. This is mainly due to difficulties of performing absolute laboratory measurements on the dipole moment in the presence of an ionic charge, small radiative absorption in dilute ionic targets, and long natural lifetimes of rotational levels. Recently, cryogenic storage rings for fast ion beams were taken in operation [4, 5] that allow the low-lying rotational levels in small molecular ions to relax by spontaneous emission toward equilibrium with a low-temperature blackbody radiation field [6]. In this Letter, we show that near-threshold photodetachment can be used to follow the in-vacuo rotational relaxation over times long compared to the natural lifetime of the first excited rotational level, and obtain Einstein coefficients for the lowest rotational transitions of the OH^- molecular anion. The measured electric dipole moment differs significantly from the theoretical values available.

Photodetachment experiments on molecular anions reveal a wealth of information on their structure and reactive dynamics. At photon energies close to the electron binding energy, the detachment cross section is a powerful probe for the internal states of the anion and the neutral daughter molecule as well as for the interaction of the outgoing low-energy electron with the neutral molecule. With its simple rotational structure in the $^1\Sigma^+$ ground state, OH^- has been intensely studied, a partic-

ular focus being the strong deviations from the Wigner threshold law in the photon energy dependence [7, 8]. Although until now significant uncertainties remain in predicting the cross sections, rotational level distributions in the anion have been characterized using the threshold structure [9, 10]. In a cold ion-trap environment, near-threshold photodetachment was applied as a method for rotational thermometry on OH^- anions under buffer-gas cooling [11, 12]. In these studies, the relative photodetachment cross-sections for the various initial and final state dependent thresholds were the main uncertainty in deconvoluting the rotational population fractions of OH^- from the measured photodetachment rates. In the present work we find that probing the radiative rotational relaxation of OH^- offers a way to obtain the convolution parameters of near-threshold photodetachment thermometry consistently on an experimental basis. Hence, in addition to the rotational lifetime measurements, we also determine relative photodetachment cross sections over a sample of near-threshold energies for individual rotational levels of OH^- .

In the present experiment, a beam of OH^- anions from a Cs sputter ion source (expected rotational temperature of a few thousand K [13]) is accelerated to 60 keV and injected into the cryogenic storage ring CSR [5]. About 10^7 ions are stored at an ambient temperature near 6 K and a residual gas density corresponding to $< 10^{-14}$ mbar room-temperature pressure. The ion storage time up to 1200 s covers the spontaneous decay of low-lying excited J levels of OH^- (~ 21 s and ~ 190 s for $J = 2$ and 1, respectively, while vibrations radiatively decay within < 1 s [14]). In a field-free straight section, laser beams are overlapped with the ion beam in co-propagating direction at a grazing angle of 3.4° . With laser and ion beam diameters of ~ 7 mm and

~ 30 mm, respectively, the interaction zone is ~ 50 cm long. The fast particles neutralized by photodetachment leave the closed orbit of the CSR and are counted by a large microchannel plate detector ~ 3 m downstream from the interaction region. A continuous-wave helium–neon (HeNe) laser at 633 nm with an effective power of 0.7 mW in the interaction region yields a steady small rate of photodetachment events. Doppler-shifted to the OH^- rest-frame its wavenumber is $\tilde{\nu}_r = 15\,754\text{ cm}^{-1}$, which is $\sim 1000\text{ cm}^{-1}$ above the first $\text{OH}^- (J=0)$ detachment threshold ($\tilde{\nu}_{\text{EA}} = 14\,741.0\text{ cm}^{-1}$) corresponding to the ground-state electron affinity [9, 10]. Measurements with buffer-gas cooled OH^- ions [15] near $15\,106\text{ cm}^{-1}$ and $15\,803\text{ cm}^{-1}$ showed that the photodetachment cross section is independent (within $\sim 10\%$) of the rotational temperature between 8 K and 300 K. Given these small variations of the photodetachment cross section with J , we use the photodetachment rate at $\tilde{\nu}_r$ as a reference signal for the number of OH^- ions in the laser interaction zone. The decay of this signal as a function of time is close to exponential with a time constant of $607(2)$ s at >150 s (only $J=0$ and 1 surviving). By searching for a component in this signal due to the $J=1$ decay, we find that the relative difference between the photodetachment cross sections of these two states is $<3\%$.

With the signal at $\tilde{\nu}_r$ for normalization, we measure the neutral rates from a second, probing laser. At similar interaction geometry as the HeNe reference laser, pulses with ~ 0.5 mJ, 3–5 ns duration and a repetition rate of 20 s^{-1} are applied by a tunable pulsed optical parametric oscillator (OPO) laser (EKSPLA NT342B). Close to the excited- J photodetachment thresholds, up to 10 probing wave numbers $\tilde{\nu}_k$ ($k = 1 \dots 10$, given in the OH^- rest-frame) are used. The neutrals reach the detector within $\sim 5\text{ }\mu\text{s}$ after the laser pulses, reflecting the particle flight times. Their counts in a suitable delay window are accumulated as the signal $N(\tilde{\nu}_k, t)$, where t is the time after the ion beam injection. Similarly, the counts due to the HeNe laser are accumulated during the breaks between the laser pulses and recorded as the reference $N(\tilde{\nu}_r, t)$. Laser pulsing starts few ms after injection. Probing wavenumbers $\tilde{\nu}_k$ are cycled through with typically 100 laser pulses at a single value. The ion beam was dumped 31 s, 300 s or 1200 s after injection. For a run, many of such injections and observation periods were repeated. The starting value of the $\tilde{\nu}_k$ cycle was varied to realize a two-dimensional spectroscopy scheme that applies all probing wave numbers to all beam storage times with a suitable time binning.

For the design of the experiment and the basic understanding of its results, modeling of OH^- near-threshold photodetachment [9, 16] was crucial. Starting from $\text{OH}^- (J)$, s -wave photodetachment can leave the OH radical ($X^2\Pi$) in up to eight final levels, each forming a threshold j at wave number $\tilde{\nu}_j$. (For $J=0$ only three thresholds are allowed.) The near-threshold de-

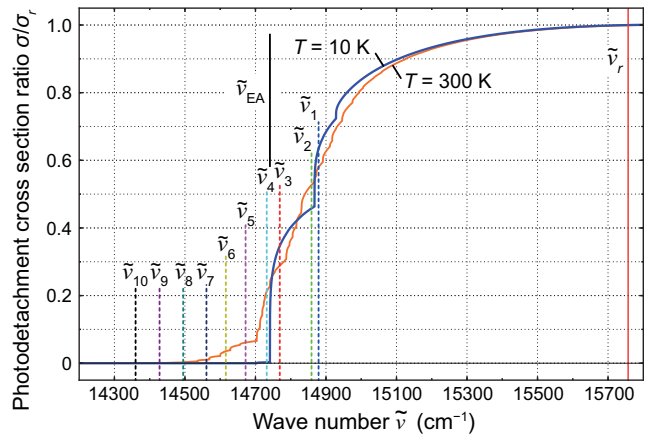


FIG. 1. Near-threshold photodetachment cross section of OH^- modeled by $\sigma_T(\tilde{\nu}; T) = \sum_J p_J(T) \sigma_J(\tilde{\nu})$ with $\sigma_J(\tilde{\nu})$ for $a = 0.20, b = -2.8$ and for $T = 10\text{ K}$ and 300 K as labeled. The reference cross section is $\sigma_r = \sigma_{J=0}(\tilde{\nu}_r)$ at the HeNe laser wave number (full vertical mark; see the text). Probing wave numbers $\tilde{\nu}_k$ are indicated by dashed marks.

tachment rate is described [17] by a Wigner-type dependence $I_j(\tilde{\nu} - \tilde{\nu}_j)^a$ where, in laser measurements just above threshold, appropriate values of a were found to vary from one threshold to the next with a typical range of $a \approx 0.20 \dots 0.25$. The threshold intensities I_j follow from the angular momenta and the OH fine structure mixing [10, 17], in reasonable agreement with the observations. Much less is known about the validity of the threshold power law at higher above-threshold photon energies ($\tilde{\nu} - \tilde{\nu}_j$), which in photodetachment thermometry can reach up a few hundred cm^{-1} . Our data analysis is largely independent of a photodetachment cross section model and we obtain the J -dependent relative cross sections from the time dependence at the various probing wave numbers $\tilde{\nu}_k$. We have to relate only one of the J -dependent cross sections at a single $\tilde{\nu}_k$ to the reference rate via the cross section model. Moreover, unresolved contributions of higher J (≥ 4) are included based on the model results. Specifically the analytical model for a threshold j is chosen as $\sigma_j(\tilde{\nu}) = \hat{I}_j(\tilde{\nu} - \tilde{\nu}_j)^a (\tilde{\nu}/\tilde{\nu}_j)^{b-a}$ with $\hat{I}_j = I_j/(2J+1)$ [18]. A factor of power $b-a$ is introduced to model cross section deviations from the threshold law at higher $\tilde{\nu}$. Only few data [15, 27] are available for the cross section in this $\tilde{\nu}$ range and indicate a maximum at, roughly, $16\,000\text{ cm}^{-1}$. We choose $a = 0.20$ and $b = -2.8$ for a model approximating the photon energy dependence.

The cross section model for $\text{OH}^- (J)$ is obtained as $\sigma_J(\tilde{\nu}) = \sum_{j(J)} \sigma_j(\tilde{\nu})$ where $j(J)$ denotes all thresholds for a given J . For OH^- with a rotational temperature T the cross section (Fig. 1) is the average over $\sigma_J(\tilde{\nu})$ with the population probabilities p_J . For $T = 10\text{ K}$, it is dominated by $J = 0$ ($p_0 = 0.987$) with a rise at $\tilde{\nu}_{\text{EA}}$ followed by two further thresholds within the next

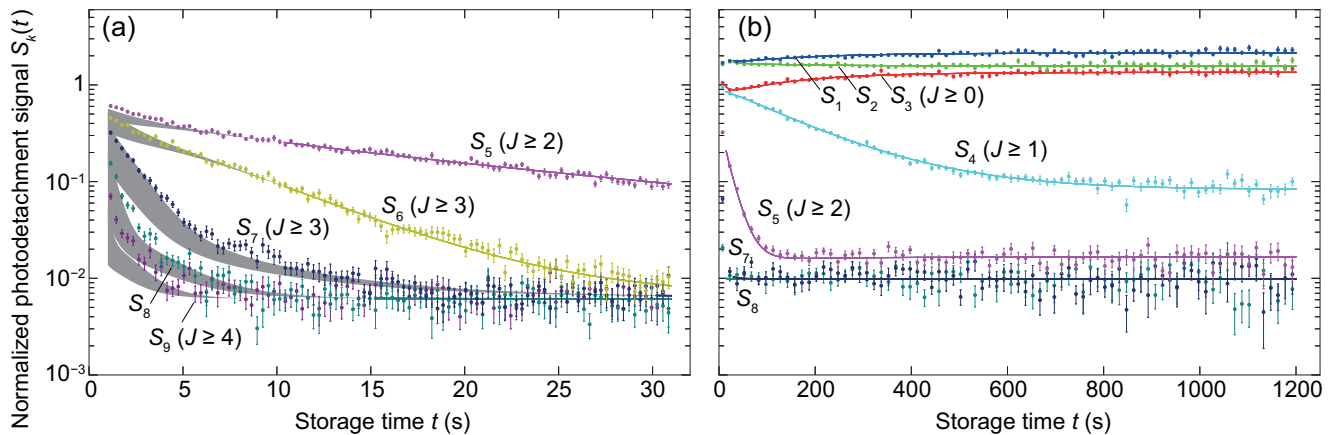


FIG. 2. Photodetachment signals $S_k(t) = N(\tilde{\nu}_k, t)/N(\tilde{\nu}_r, t)$ as functions of the ion storage time for two sample runs with 1151 (a) and 38 (b) injections. Ranges of J -levels contributing to the signals are marked. Data points represent the measured count ratios and their 1σ uncertainties. The full lines show a fit to the signals of all runs using the modeled photodetachment cross sections and level populations. In (a) the shaded areas indicate the model variation with T_0 at the short times when the data were excluded from the fit (see text).

200 cm^{-1} . Higher J levels populated at $T = 300$ K lead to a broadening of the threshold structures, while from ~ 600 cm^{-1} above $\tilde{\nu}_{\text{EA}}$ the cross sections are largely independent of T and of J .

Among the probe wave numbers, $\tilde{\nu}_1 \dots \tilde{\nu}_3$ lie well above $\tilde{\nu}_{\text{EA}}$ (Fig. 1) and, thus, yield contributions from all $J \geq 0$. Other $\tilde{\nu}_k$ successively exclude low- J levels; contributing J 's are, e.g., $J \geq 1$ for $\tilde{\nu}_4$ and $J \geq 2$ for $\tilde{\nu}_5$. Signals $S_k(t) = N(\tilde{\nu}_k, t)/N(\tilde{\nu}_r, t)$, shown in Fig. 2, are obtained by normalizing the counts $N(\tilde{\nu}_k, t)$ to the reference $N(\tilde{\nu}_r, t)$. A short run up to 31 s, using $\tilde{\nu}_5 \dots \tilde{\nu}_9$, shows the successive cooling of higher rotational levels. After the fast decay of $J \geq 4$ ($t \gtrsim 10$ s), S_6 essentially shows the relaxation of $J = 3$. Similarly, S_5 at later times ($\gtrsim 30$ s) represents the $J = 2$ decay. In a long run up to 1200 s, S_4 for $t \gtrsim 200$ s represents the pure $J = 1$ decay. Furthermore, the signals $S_1 \dots S_3$ clearly show the different J contributions by their characteristic time dependences consistent with S_4 and S_5 , in particular.

The normalized signals represent a convolution of the time-dependent J -level populations p_J with a matrix representing the relative photodetachment cross sections at the probing wave numbers: $S_k(t) = S_0 \sum_J p_J(t) \phi_k \sigma_J(\tilde{\nu}_k)/\sigma_r$. Factors ϕ_k close to 1 describe the small relative variations of the OPO laser flux over $\tilde{\nu}_k$ (known within $\sim 3\%$). The OH^- radiative relaxation can be well described by only a few parameters: the Einstein coefficients A_J for transitions $J \rightarrow J - 1$, the photon occupation numbers $n(\tilde{\nu}_J)$ of the ambient radiation field at the transition energies $\tilde{\nu}_J$ for transitions $J \rightarrow J + 1$, and the initial populations p_J^0 of the rate model [18]. An overall scaling parameter S_0 (in the range of 3.4 to 4.4) takes into account the integrated powers and the slightly different overlaps of the two laser beams.

The signals $S_k(t)$ were fitted by a single model simul-

taneously for all runs. We assume that the $n(\tilde{\nu}_J)$ are given by a radiative temperature T_r according to Bose-Einstein statistics. The populations p_J^0 from the excitation in the ion source are described by a temperature T_0 . We independently varied in the fit all A_J for $J \leq 3$. At the various $\tilde{\nu}_k$, the signal variations differently reflect the radiative time constants and the J -dependent photodetachment cross sections $\sigma_J(\tilde{\nu}_k)/\sigma_r$. Hence, the relative cross sections can also be obtained.

We fit $S_{1,2}$ for $t > 30$ s and S_3 to S_6 for $t > 10$ s to determine relative σ_J values for $J = 0$ to 3. The time limits are set to safely ensure the decay of higher- J levels. On the other hand, the radiative lifetimes of $J = 1$ to 3 are sensitively probed. For fitting S_0 , one of the relative photodetachment cross sections, for which we chose $\sigma_{J=0}(\tilde{\nu}_3)/\sigma_r$, has to be set to its calculated value. In S_7 to S_{10} , contributions from various higher J overlap at shorter times. We do not fit these short-time data, but only compare them to the model using the calculated $\sigma_J(\tilde{\nu}_k)/\sigma_r$. The higher- J lifetimes are set according to the relation $A_J = 16\pi^3 \tilde{\nu}_{J-1}^3 \mu_{0,J}^2 / 3\epsilon_0 h(2J+1)$ [23] using the dipole moment $\mu_{0,J \geq 3}$ from the fitted $J = 3$ lifetime. The backgrounds in these data are fitted for $t > 15$ s ($t > 30$ s for S_7). Separate fits were performed setting the start temperature T_0 between 1000 K and 6000 K. Within the fitted time ranges the model curves and the fitted parameters remain essentially unchanged. In the short-time ranges excluded from the fits the results vary significantly. This is indicated by shaded areas in Fig. 2(a). Their upper edges, representing the model for $T_0 = 6000$ K, yield best agreement with the data. Hence, we give the results for the fit at $T_0 = 6000$ K and consider the estimated parameter variations over a range of ± 2000 K in T_0 as a systematic uncertainty. The reduced mean-squared residuals χ_r^2 were close to 1.30 in all cases.

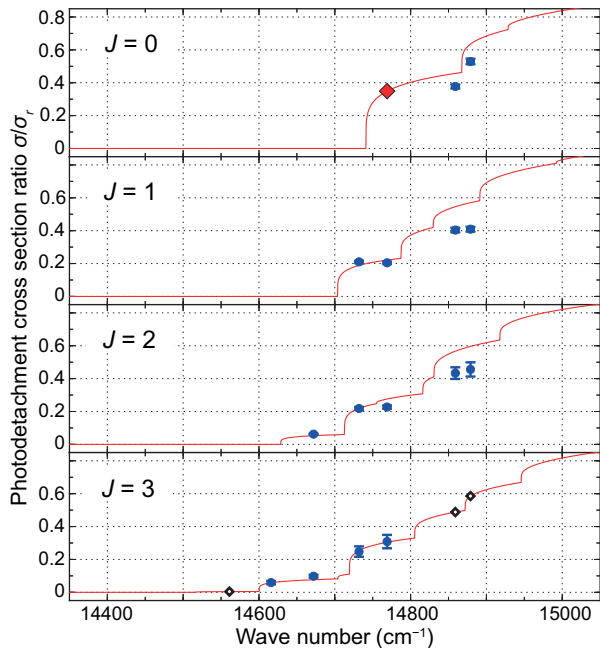


FIG. 3. Near-threshold photodetachment cross section ratios $\sigma_J(\tilde{\nu})/\sigma_r$ of OH^- for the probing lines ($\tilde{\nu} = \tilde{\nu}_k$) determined from the fit (filled symbols with overall 1σ , statistical and systematic uncertainties) and the model with $a = 0.20$, $b = -2.8$ (full lines). Open diamonds mark theoretical values of $\sigma_J(\tilde{\nu}_k)/\sigma_r$ for the channels where separate features cannot be identified in the data. The model value of $\sigma_{J=0}(\tilde{\nu}_3)/\sigma_r$ serving as a reference (see text) is marked by the large diamond.

Two further experimental features were included in the fit. First, a small fraction of $^{17}\text{O}^-$ ions of $(1.7 \dots 5.9) \times 10^{-3}$ [18] occurred in the stored OH^- beam and, for the O^- electron affinity near 11784.7 cm^{-1} [28], led to a small constant neutralization background even for the probing lines far below the OH^- threshold. It was considered as a constant background in $S_k(t)$ with independent values for different runs. Moreover, reflection of laser light at the downstream vacuum window produced a small additional probing-light component Doppler-shifted by $\tilde{\nu}'_k - \tilde{\nu}_k \approx +80 \text{ cm}^{-1}$. This yields a small contribution from $J = 0$ ions in S_5 (probing $J \geq 2$) slightly shifting the S_5 equilibrium level in Fig. 2(b). The weak, Doppler-shifted reflected lines ($\tilde{\nu}'_k$) are consistently included in the model (with theoretical $\sigma_J(\tilde{\nu}'_k)/\sigma_r$) and the reflection factors (up to a few percent) are allowed to vary between different runs. In the fit results, systematic uncertainties due to the starting temperature T_0 have a few-percent effect on the relative cross sections, while they are negligible for the radiative decay and the equilibrium population. The estimated limits for rotational variations of the reference photodetachment cross section and differences in depleting the various J -levels by laser photodetachment introduce [18] systematic uncertainties on the radiative decay rates which are included in the

TABLE I. Einstein coefficients, natural lifetimes τ_J and the corresponding transition dipole moments measured for OH^- rotational states with the combined statistical and systematic uncertainty (1σ confidence level).

	$J = 1$	$J = 2$	$J = 3$	unit
A_J	0.00517(18)	0.0478(48)	0.189(13)	s^{-1}
$\tau_J = A_J^{-1}$	193(7)	20.9(2.1)	5.30(37)	s
μ_0	0.970(17)	0.952(48)	0.997(35) ^a	D

^a Value used for $\mu_{0,J \geq 3}$

overall uncertainty limits of the results.

The fits shown in Fig. 2 yield precise details on the radiative equilibrium in the low-level blackbody field of the CSR, the relative probing cross sections and the radiative decay rates of the OH^- ion. From the fitted photon occupation number at the $J = 0 \rightarrow 1$ transition frequency in OH^- (37.47 cm^{-1}), we obtain an effective radiative temperature of $T_r = 15.1(1) \text{ K}$. Considering the CSR vacuum-chamber temperature [5] near 6 K, the effective relative contribution from room-temperature surfaces to the radiation field is found [18] to be $5.7(2) \times 10^{-3}$.

The fit results for the state-selected relative photodetachment cross sections at the various probe wave numbers are shown in Fig. 3. It is clearly visible that the simple model is inappropriate for the probing energies of 100 cm^{-1} or more above the lowest thresholds in $J = 0$ to 2. As a simple change of the common exponent a of all threshold laws does not improve the overall agreement, the results call for more detailed cross-section calculations beyond simple power-law models. But the experimental cross section ratios (see listing in Ref. [18]) can directly serve for future photodetachment thermometry, deducing rotational populations from relative photodetachment rates on a theory-independent basis. This will include ion trap experiments such as those of Refs. [11, 12], where photodetachment thermometry serves to study cold inelastic collisions by laser depletion of rotational levels.

Results for the Einstein coefficients and the molecular dipole moment are listed in Table I. To our best knowledge, direct in-vacuo lifetime measurements on low-lying, purely rotationally excited states in small molecules have not been reported previously. As expected at the given accuracy, the molecular dipole moments extracted from A_J assuming the elementary Hönl-London factors are compatible among each other within experimental uncertainties. The weighted average of $\mu_0 = 0.982(15) \text{ D}$ can be compared to calculations of the OH^- dipole moment. Values at the equilibrium internuclear distance are 1.050 to 1.072 D in earlier [25] and 1.10 D in recent work [29]. Taking the dipole moment function of Ref. [25], vibrational averaging reduces μ_0 by at most 0.04 D ($\mu_0 = 1.037 \text{ D}$ [18]). Hence, we find that cur-

rent theory overestimates the OH^- dipole moment by $(5.3 \pm 1.5)\%$ and underestimates the OH^- rotational lifetimes by about $(10 \pm 3)\%$.

In the described time-dependent near-threshold photodetachment spectroscopy using a cryogenic storage ring, the well-understood dynamics of in-vacuo radiative relaxation allowed us to clearly identify the contributions of single rotational levels. This single-level sensitivity will be useful in the future to probe rotational population changes by in-ring molecular collisions. Moreover, a method was demonstrated to perform precise laboratory measurements of natural lifetimes and line intensities for extremely slow, purely rotational transitions in molecular ions. Rotational lifetimes from such measurements add a further, so far unavailable experimental benchmark for quantum chemical calculations. Further improvements of the accuracy and applications to anionic molecules with more complicated rotational level structures can be envisaged.

Support by the Max Planck Förderstiftung is gratefully acknowledged. F. G., E. A. G., A. P. O. and H. K. were supported by the European Research Council under Grant Agreement No. StG 307163.

* Email: cmeyer@mpi-hd.mpg.de

† Deceased.

- [1] E. Herbst, *Nature* **289**, 656 (1981).
- [2] S. Petrie and E. Herbst, *Astrophys. J.* **491**, 210 (1997).
- [3] M. C. McCarthy, C. A. Gottlieb, H. Gupta, and P. Thaddeus, *Astrophys. J.* **652**, L141 (2006).
- [4] E. Bäckström, D. Hanstorp, O. M. Hole, M. Kaminska, R. F. Nascimento, M. Blom, M. Björkhage, A. Källberg, P. Löfgren, P. Reinhed, S. Rosén, A. Simonsson, R. D. Thomas, S. Mannervik, H. T. Schmidt, and H. Cedergren, *Phys. Rev. Lett.* **114**, 143003 (2015).
- [5] R. von Hahn, A. Becker, F. Berg, K. Blaum, C. Breitenfeldt, H. Fadil, F. Fellenberger, M. Froese, S. George, J. Göck, M. Grieser, F. Grussie, E. A. Guerin, O. Heber, P. Herwig, J. Kartheim, C. Krantz, H. Kreckel, M. Lange, F. Laux, S. Lohmann, S. Menk, C. Meyer, P. M. Mishra, O. Novotný, A. P. O'Connor, D. A. Orlov, M. L. Rappaport, R. Repnow, S. Saurabh, S. Schippers, C. D. Schröter, D. Schwalm, L. Schweikhard, T. Sieber, A. Shornikov, K. Spruck, S. Sunil Kumar, J. Ullrich, X. Urbain, S. Vogel, P. Wilhelm, A. Wolf, and D. Zajfman, *Rev. Sci. Instrum.* **87**, 063115 (2016).
- [6] A. P. O'Connor, A. Becker, K. Blaum, C. Breitenfeldt, S. George, J. Göck, M. Grieser, F. Grussie, E. A. Guerin, R. von Hahn, U. Hechtfisher, P. Herwig, J. Kartheim, C. Krantz, H. Kreckel, S. Lohmann, C. Meyer, P. M. Mishra, O. Novotný, R. Repnow, S. Saurabh, D. Schwalm, K. Spruck, S. Sunil Kumar, S. Vogel, and A. Wolf, *Phys. Rev. Lett.* **116**, 113002 (2016).
- [7] P. C. Engelking and D. R. Herrick, *Phys. Rev. A* **29**, 2425 (1984).
- [8] J. R. Smith, J. B. Kim, and W. C. Lineberger, *Phys. Rev. A* **55**, 2036 (1997).
- [9] P. A. Schulz, R. D. Mead, P. L. Jones, and W. C. Lineberger, *J. Chem. Phys.* **77**, 1153 (1982).
- [10] F. Goldfarb, C. Drag, W. Chaibi, S. Kröger, C. Blondel, and C. Delsart, *J. Chem. Phys.* **122**, 014308 (2005).
- [11] R. Otto, A. von Zastrow, T. Best, and R. Wester, *Phys. Chem. Chem. Phys.* **15**, 612 (2013).
- [12] D. Hauser, S. Lee, F. Carelli, S. Spieler, O. Lakhmanskaya, E. S. Endres, S. S. Kumar, F. Gianturco, and R. Wester, *Nat. Phys.* **11**, 467 (2015).
- [13] S. Menk, S. Das, K. Blaum, M. W. Froese, M. Lange, M. Mukherjee, R. Repnow, D. Schwalm, R. von Hahn, and A. Wolf, *Phys. Rev. A* **89**, 022502 (2014).
- [14] Z. Amitay, D. Zajfman, and P. Forck, *Phys. Rev. A* **50**, 2304 (1994).
- [15] P. Hlavenka, R. Otto, S. Trippel, J. Mikosch, M. Weidemüller, and R. Wester, *J. Chem. Phys.* **130**, 061105 (2009).
- [16] H. Hotop, T. A. Patterson, and W. C. Lineberger, *J. Chem. Phys.* **60**, 1806 (1974).
- [17] P. A. Schulz, R. D. Mead, and W. C. Lineberger, *Phys. Rev. A* **27**, 2229 (1983).
- [18] See Supplementary Material at ... for methods, data analysis details, and numerical results, which includes Refs. [19–26].
- [19] J. D. Rudmin, L. P. Ratliff, J. N. Yukich, and D. J. Larson, *J. Phys. B: At. Mol. Opt. Phys.* **29**, L881 (1996).
- [20] J. P. Maillard, J. Chauville, and A. W. Mantz, *J. Mol. Spectrosc.* **63**, 120 (1976).
- [21] S. Gewurtz, H. Lew, and P. Flainek, *Can. J. Phys.* **53**, 1097 (1975).
- [22] F. Breyer, P. Frey, and H. Hotop, *Z. Phys. A* **300**, 7 (1981).
- [23] P. F. Bernath, *Spectra of Atoms and Molecules*, 2nd ed. (Oxford University Press, New York, 2005).
- [24] Y.-P. Chang, F. Filsinger, B. G. Sartakov, and J. Küpper, *Comp. Phys. Commun.* **185**, 339 (2014).
- [25] H. Werner, P. Rosmus, and E. Reinsch, *J. Chem. Phys.* **79**, 905 (1983).
- [26] G. L. Molnár and R. B. Firestone, in *Handbook of Nuclear Chemistry*, edited by A. Vértes, S. Nagy, Z. Klencsár, R. G. Lovas, and F. Rösch (Springer US, 2011) pp. 475–610.
- [27] L. M. Branscomb, *Phys. Rev.* **148**, 11 (1966).
- [28] C. Blondel, W. Chaibi, C. Delsart, C. Drag, F. Goldfarb, and S. Kröger, *Eur. Phys. J. D* **33**, 335 (2005).
- [29] B. S. D. R. Vamhindi and M. Nsangou, *Mol. Phys.* **114**, 2204 (2016).

Online Supplementary Material

Radiative rotational lifetimes and state-resolved relative detachment cross sections from photodetachment thermometry of molecular anions in a cryogenic storage ring

C. Meyer¹, A. Becker¹, K. Blaum¹, C. Breitenfeldt^{1,2}, S. George¹, J. Göck¹, M. Grieser¹, F. Grussie¹, E. A. Guerin¹, R. von Hahn¹, P. Herwig¹, C. Krantz¹, H. Kreckel¹, J. Lion¹, S. Lohmann¹, P. M. Mishra¹, O. Novotný¹, A. P. O'Connor¹, R. Repnow¹, S. Saurabh¹, D. Schwalm^{1,3}, L. Schweikhard², K. Spruck^{1,4}, S. Sunil Kumar¹, S. Vogel¹, and A. Wolf¹

¹Max-Planck-Institut für Kernphysik, 69117 Heidelberg, Germany; ²Institut für Physik, Ernst-Moritz-Arndt-Universität Greifswald, D-17487 Greifswald, Germany; ³Weizmann Institute of Science, Rehovot 76100, Israel; ⁴Institut für Atom- und Molekülphysik, Justus-Liebig-Universität Gießen, D-35392 Gießen, Germany

In this Supplementary Material, we collect additional information about the methods of the measurement and data analysis. In the final section, we make some results available in numerical form.

Photodetachment modeling

Our modeling of the OH⁻ near-threshold photodetachment cross sections is based on the work by Schulz *et al.* [1], Rudmin *et al.* [2], and Goldfarb *et al.* [3]. Earlier research on the topic is cited in these publications. The OH⁻ anion is assumed to be in the vibrational ground state. Its state is specified by the rotational quantum number J'' (denoted by J in the main article) and the parity $(-1)^{J''}$. In the neutral OH product, two levels exist for a given total angular momentum J' and parity. These levels arise from the fine-structure interaction and the angular momentum coupling in the $X^2\Pi$ state of OH. The energetically lower levels for a given J' are denoted as the F1 levels and the higher ones as the F2 levels (a number parameter $\alpha = 1, 2$ for F1 and F2, respectively, is used as well). The intensity of the threshold (wave number $\tilde{\nu}_i$) is described [1, 3] by an expression I_j containing the squares of a linear combination of relevant transition matrix elements, where j represents the set of labels (J', α, J'') for a specific threshold. As discussed in the main text, I_j is multiplied by a threshold law of form $(\tilde{\nu} - \tilde{\nu}_j)^a$ with a positive fractional exponent a to describe the energy dependence of the photodetachment intensity. We choose to model the photodetachment cross section of a threshold j by $\sigma_j(\tilde{\nu}) = \hat{I}_j(\tilde{\nu} - \tilde{\nu}_j)^a(\tilde{\nu}/\tilde{\nu}_j)^{b-a}$ with the parameters $a = 0.20 \dots 0.25$ and $b = -2.8$ discussed in the main text. The cross-section intensity factors \hat{I}_j are related to the

TABLE SI. Spectroscopic constants applied in the model calculations for OH (Table IV of Ref. [4]) and OH⁻ (Table II of Ref. [5]; in cm⁻¹) in the ground electronic and vibrational levels.

	OH	OH ⁻
\tilde{E}_{EA}	14 741.0 ^a	
A_0	-139.18	
B_0	18.550	18.741
D_0	1.916×10^{-3}	2.052×10^{-3}
$P(0)$	0.234	
$Q_0(0)$	-0.039	

^a Rounded value keeping agreement with Refs. [3, 5].

threshold intensity I_j calculated in the literature [1, 3] as

$$\hat{I}_j = I_j / (2J'' + 1) \quad (\text{S1})$$

considering the average over degenerate states for the initial level OH⁻(J''). The threshold wave numbers $\tilde{\nu}_j$ are considered below.

In the intermediate-coupling model used, the OH energy levels are described by a superposition of Hund's case (a) states ${}^2\Pi_{\Omega'}$ where Ω' is the absolute value of the projection of the total electronic angular momentum on the internuclear axis. Following the well established theory for diatomic hydrides with a ${}^2\Pi$ ground state, with particular reference to the treatment of HF⁺ (isoelectronic to OH) by Gewurtz *et al.* [6], and using the molecular constants [4] listed for OH in Table SI, the energies of the F1 and F2 states with both parities (e, f) are obtained by ($\Lambda = 1$ in Ref. [6])

$$\begin{aligned} \tilde{E}_{J',1}^{\text{OH}} &= \tilde{E}_{\text{F1}} = B_0[(J' + 1/2)^2 - 1 - X/2] - D_0 J'^4 \pm \Delta \tilde{E}_{fe}^{(1)}/2, \\ \tilde{E}_{J',2}^{\text{OH}} &= \tilde{E}_{\text{F2}} = B_0[(J' + 1/2)^2 - 1 + X/2] - D_0 (J' + 1)^4 \pm \Delta \tilde{E}_{fe}^{(2)}/2, \end{aligned} \quad (\text{S2})$$

where $Y = A_0/B_0$ (< 0 for OH), and

$$X = [4(J' + 1/2)^2 + Y(Y - 4)]^{1/2}. \quad (\text{S3})$$

The lambda doubling is taken into account by the parameters [6]

$$\Delta \tilde{E}_{fe}^{(1,2)} = \mp (J' + 1/2) \{ (\mp 1 + 2/X - Y/X)[P_0/2 + Q_0(0)] + 2Q_0(0)(J' + 1/2)(J' + 3/2)/X \}, \quad (\text{S4})$$

where the upper (lower) signs hold for the indices 1 (2), respectively, and $\Delta \tilde{E}_{fe} = \tilde{E}_f - \tilde{E}_e$. The e states have parity $(-1)^{J'-1/2}$ and the f states parity $-(-1)^{J'-1/2}$. The lowest OH level is

$\tilde{E}_0^{\text{OH}} = \tilde{E}_{3/2,1}^{\text{OH}}$ with odd parity (i.e., the e level). The mixing coefficient

$$\kappa = [(X - 2 + Y)/2X]^{1/2} \quad (\text{S5})$$

governs the amplitudes of the Hund's-case-(a) (fixed Ω') states in the F1 and F2 levels, further discussed below. In the case of OH with $Y < 0$ the lower-energy (F1) states have dominantly character $\Omega' = 3/2$ and the higher-energy (F2) states dominantly $\Omega' = 1/2$.

The threshold photon energy $\tilde{\nu}_j$ is obtained from the OH^- and OH level energies and the electron affinity \tilde{E}_{EA} (see Table SI) as

$$\nu_j = \tilde{E}_{J',\alpha}^{\text{OH}} - \tilde{E}_0^{\text{OH}} + \tilde{E}_{\text{EA}} - \tilde{E}_{J''}^{\text{OH}^-}. \quad (\text{S6})$$

The OH^- energy levels, considering the molecules to be in the vibrational ground state, are described by the linear non-rigid rotor model using

$$\tilde{E}_{J''}^{\text{OH}^-} = B_0 J''(J'' + 1) - D_0 J''^2(J'' + 1)^2. \quad (\text{S7})$$

For the dominant s wave photodetachment only considered here, the required OH parity is $-(-1)^{J''}$, and $\tilde{E}_{J',\alpha}^{\text{OH}}$ refers to the level of this parity. For $J'' = 0$ the lowest s -wave threshold leads to the level $\tilde{E}_{3/2,1}^{\text{OH}}$ with odd parity and hence the wave number of this threshold equals \tilde{E}_{EA} .

The calculation of the intensities I_j proceeds by first considering the photoexcitation of an intermediate state (complex) of negative total charge with the angular momentum quantum number J_C . This state evolves to possible final states of OH with labels (J', α) and an s -wave electron by recoupling of angular momenta and their projection on the internuclear axis. The angular momentum J_C follows the dipole transition selection rules ($J_C = J''$ or $J'' \pm 1$) while the spin $1/2$ carried away by the outgoing electron then allows $J' = J'' \pm 1/2$ or $J'' \pm 3/2$ ($J_C = J' \pm 1/2$). The J_C dependence of the phototransition is expressed by a constant radial transition dipole moment and the Hönl-London factors. In the intensity factor, pathways corresponding to different J_C and Ω' interfere as expressed by appropriate amplitudes for each (J', α) final state.

In their Eqs. (3) to (6) Goldfarb *et al.* [3] correct a small typographic error of Ref. [1] and list the results of the calculation. We use these expressions setting $I_j = I$ for the quantum numbers corresponding to threshold j . Here, mixing coefficients c_1 and c_2 specify the final levels (J', α) in terms of their Hund's-case-(a) components. Specifically, the state amplitudes are represented by c_1 for the basis state ${}^2\Pi_{1/2}$ and by c_2 for the basis state ${}^2\Pi_{3/2}$. Goldfarb *et al.* [3] emphasize the importance of a proper phase choice for these mixing coefficients and mention a check regarding the intensities of the various branches j . For the state amplitudes expressions are given by Schulz

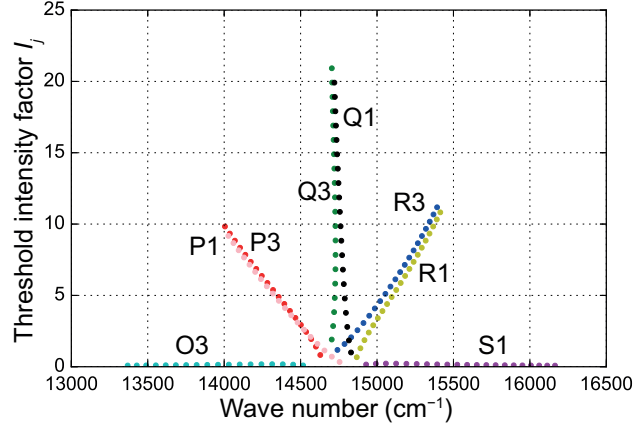


FIG. S1. Intensity factors I_j for the s -wave photodetachment thresholds of the OH^- rotational levels up to $J'' = 20$.

et al. [1], Eq. (5), which regarding absolute values correspond to the coefficient given in our Eq. (S5). However, we found it essential to verify the branch intensities regarding the relative signs of c_1 and c_2 . For our model calculations, the state amplitudes were then, for an F1 ($\alpha = 1$) level, set as

$$c_1 = c_1^{(F1)} = \kappa, \quad c_2 = c_2^{(F1)} = -\sqrt{1 - \kappa^2} \quad (\text{S8})$$

while for an F2 ($\alpha = 2$) level,

$$c_1 = c_1^{(F2)} = \sqrt{1 - \kappa^2}, \quad c_2 = c_2^{(F2)} = \kappa \quad (\text{S9})$$

with κ from Eq. (S5). Both equations apply to the OH case ($Y < 0$). The branch intensities I_j obtained with this definition are shown in Fig. S1 and, as discussed below, fulfil the criterium formulated by Goldfarb *et al.* [3]. Hence, we find that, for OH and for the formula set of Eqs. (3) to (6) in Ref. [3], the c_1, c_2 coefficients must be chosen with *opposite* signs for the F1 state (i.e., the $\Omega' = 3/2$ dominated state). With relation to Schulz *et al.* [1], Eq. (5), we have $c_{1,2}^{(F1)} = c_{1a,2a}$ and $c_{1,2}^{(F2)} = c_{1b,2b}$ and, unlike quoted in this reference for the OH case, have to use the *upper* signs in these expressions.

In Fig. S1 we show the values of I_j obtained with Eq. (3) to (5) from Goldfarb *et al.* [3] and our Eqs. (S8,S9). As functions of the threshold energy $\tilde{\nu}_j$, the intensities are clearly grouped in branches. Their customary notation refers to the quantum number N' (total angular momentum except spin) of the respective dominant component (i.e., $N' = J' - 1/2$ for F1 levels with $\Omega' = 3/2$ main component and $N' = J' + 1/2$ for F2 levels). For a Q branch, $N' = J''$, while branches R and P are defined by $N' = J'' \pm 1$ and S and O branches by $N' = J'' \pm 2$, respectively. Branches

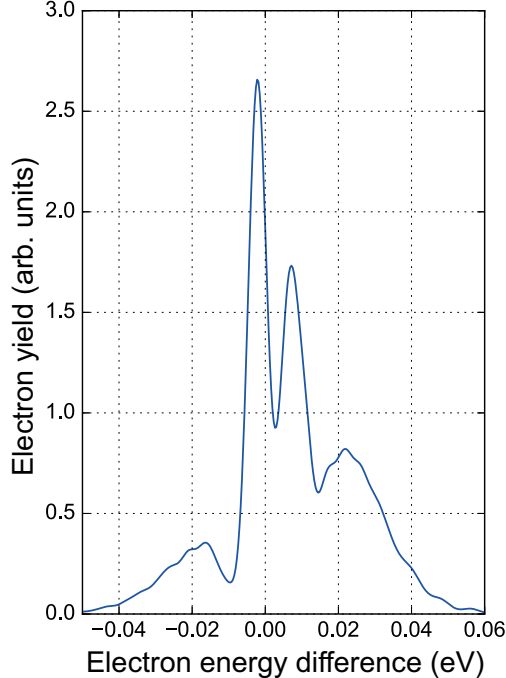


FIG. S2. Reproduction of the electron spectrum measured by Breyer *et al.* [7] for OH^- photodetachment at $\tilde{\nu} = 20492 \text{ cm}^{-1}$. Comparison to Fig. 1 of Ref. [1] shows that the result of Schulz *et al.* is precisely reproduced by our implementation of the model.

denoted as O3, P3, Q3 and R3 lead to F1 levels ($\Omega = 3/2$ dominant), while the branches P1, Q1, R1 and S1 lead to F2 levels ($\Omega = 1/2$ dominant). It is seen that, as expected, the P, Q and R branches of the F1 and F2 levels show similar behavior for high J'' , while the O3 and S1 branches keep low amplitudes for all J'' . This dramatically changes when the phases in Eqs. (S8,S9) are reversed.

The values of I_j plotted in Fig. S1 show an approximately linear increase with J'' . Hence, at excess photon energies $\tilde{\nu} - \tilde{\nu}_0$ large compared to the spacing between the rotational thresholds $\tilde{\nu}_j$, we will have a similar near-linear increase also for $I_j(\tilde{\nu} - \tilde{\nu}_j)^a \approx I_j(\tilde{\nu} - \tilde{\nu}_0)^a$. Only the division by the initial-state statistical weight, using the factors defined in Eq. (S1), avoids a drastic dependence on J'' of the cross section at high photon energies above the threshold. In previous applications [1, 3] the intensities I_j were multiplied with pure Boltzmann factors (as opposed to level population fractions) in order to obtain the J'' -dependent relative photodetachment intensities, which is consistent with our cross-section definition.

For another check, we have followed Schulz *et al.* [1] and reproduced their model of the electron spectra measured by Breyer *et al.* [7] for high excess photon energies (Fig. S2). It turned out that it is essential to apply the sign convention of Eqs. (S8,S9), together with a suitable cross-section

definition, to obtain agreement with both the experimental and the earlier model data. The model results given in Ref. [1] can be reproduced accurately with the sign convention of Eqs. (S8,S9), which thus seems to be the one used by these authors (in spite of the opposite statement near Eq. (5) of Ref. [1]).

Radiative relaxation

Molecules with infrared active modes like OH^- couple to the surrounding radiative field by emitting and absorbing photons. The rates of such processes can be described by the Einstein coefficients. We assume that the molecules are in the vibrational ground state only. Denoting in this section the OH^- quantum number by J , the level energies $\tilde{E}_J = \tilde{E}_{J''}^{\text{OH}^-}$ are given by Eq. (S6) with $J'' = J$ and the parameters from Table SI. Considering electric dipole transitions only, radiative transitions occur between adjacent J levels only and we index the transition wave numbers by the lower J : $\tilde{\nu}_J = \tilde{E}_{J+1} - \tilde{E}_J$. The radiative field is specified by the photon occupation numbers at the transition frequencies, $n(\tilde{\nu}_J)$, assuming the vacuum mode density and unpolarized conditions. If the radiation field can be characterized by a single temperature T_r , the photon occupation numbers follow the Bose-Einstein statistics,

$$n(\tilde{\nu}_J) = [\exp(hc\tilde{\nu}_J/k_B T_r) - 1]^{-1} \quad (\text{S10})$$

with the Boltzmann constant k_B . By the rotational transitions, the radiative field is sampled at the approximately equidistant wave numbers $\tilde{\nu}_J \approx 2B_0(J+1)$.

The transition rates for radiative emission *out* of a level J are given by

$$k_{J \rightarrow J-1}^{\text{em}} = A_J [1 + n(\tilde{\nu}_{J-1})] \quad (\text{S11})$$

where A_J is the Einstein coefficient for the spontaneous decay of level J :

$$A_J = (16\pi^3/3\epsilon_0 h) \tilde{\nu}_{J-1}^3 \mu_0^2 J / (2J+1) \quad (= A_{J \rightarrow J-1}). \quad (\text{S12})$$

from Ref. [8] assuming the Hönl-London factors [Eq. (9.115); Table 9.4 for R transitions]. Absorption processes *out* of J have the rate

$$k_{J \rightarrow J+1}^{\text{abs}} = A_{J+1} n(\tilde{\nu}_J) (2J+3) / (2J+1). \quad (\text{S13})$$

Together with the *in*-going processes into level J the rate equation model is obtained:

$$dp_J/dt = k_{J-1 \rightarrow J}^{\text{abs}} p_{J-1} - (k_{J \rightarrow J+1}^{\text{abs}} + k_{J \rightarrow J-1}^{\text{em}}) p_J + k_{J+1 \rightarrow J}^{\text{em}} p_{J+1}. \quad (\text{S14})$$

We integrate the differential equation system with initial populations p_J^0 and close the system by setting $p_J \equiv 0$ and $A_J \equiv 0$ for $J > J_{\max}$ as well as for $J < 0$. The used p_J^0 and, hence, p_J are normalized ($\sum_J p_J = 1$). Initial populations are defined by a Boltzmann distribution of temperature T_0 . We work at $T_0 < 6000$ K and for this upper temperature limit, $p_J < 10^{-4}$ for $J > 50$. In the model we use $J_{\max} = 50$.

The natural lifetimes $\tau_J = 1/A_J$ decrease rapidly with J . As a consequence each excited rotational state cools faster than the next lower one. With the condition $\Delta J = \pm 1$ (R transitions, only) this slows down the radiative cascade into the rotational ground state. Moreover, the higher- J states with shorter lifetime already thermalize among each other before population accumulates in the lower states. Approximately, the accumulation rate is limited by the lifetime of the lowest already thermalized level. This behavior significantly reduces the influence of the initial populations p_J^0 on those occurring after some in-vacuo relaxation time.

It should be noted that the decay constants of the J levels are not in general identical to A_J , but modified by the ambient radiation field. In particular, the decay constant of the $J = 1$ level, from finding the solution of Eq. (S14), amounts to $[1 + 4n(\tilde{\nu}_{J=0})]A_1$. Even at the present low-level cryogenic radiation field it is, thus, larger than A_1 by about 12% (see p. 10 below).

Systematic uncertainties

The systematic uncertainties of the parameters from the fit of the probing signals are determined for various influences as follows.

Starting temperature. Fit results for the starting temperatures of 4000 K and 6000 K are compared, estimating the variations of the fit parameters for a starting temperature difference of ± 2000 K around $T_0 = 6000$ K. This yields relative effects of $< 0.1\%$ for A_1 and A_2 and of 0.15% for A_3 , which are negligible w.r.t. the 1σ statistical uncertainties (1.3% for A_1 and 3% for A_2 and A_3). Similarly, the 0.03 K uncertainty of T_r is neglected. For the fitted relative detachment cross sections, the uncertainties due to the starting temperature, determined by the same method, are linearly added to the 1σ statistical uncertainty to yield a total estimated uncertainty.

Rotational variation of the reference photodetachment cross section. The effect of a J -dependence in σ_r at 15754 cm^{-1} can be estimated by considering the fit to S_4 . At $t > 150$ s, this essentially is determined by $J = 1$ photodetachment only. For the final approach to equilibrium between $J = 1$ and $J = 0$, with relative populations at $t = 150$ s of $p_1 \approx p_0 \approx 0.5$ at $t = 150$ s, the signal $S_4 \approx N_{J=1}(\tilde{\nu}_4, t) / [N_{J=1}(\tilde{\nu}_r, t) + N_{J=0}(\tilde{\nu}_r, t)]$ can be modeled explicitly, introducing a relative

cross section difference $\eta_r = \sigma_r^{J=1}/\sigma_r^{J=0} - 1$. Fitting this model to the data using different near-zero values of η_r yields a sensitivity of $\Delta A_1/\Delta\eta_r = +1.45 \times 10^{-3} \text{ s}^{-1}$. We also searched for a component describing the $J = 1$ decay in the reference signal $N(\tilde{\nu}_r, t)$. This component has a decay rate of $[1 + 4n(\tilde{\nu}_{J=0})]A_1$ according to the radiative model. The search yields $\eta_r = -0.01(2)$. Hence, the systematic effect on A_1 due to the J -dependence of σ_r is estimated as $\Delta A_1 = -1.5(3.0) \times 10^{-5} \text{ s}^{-1}$. We choose to keep the value from the overall fit, $A_1 = 5.17(7) \times 10^{-3} \text{ s}^{-1}$, and linearly add a systematic uncertainty of $\pm 1\%$ due to the J -dependence of σ_r . The previous measurement in Ref. [9] indicates that the photodetachment cross section is independent of J for $J = 0$ to 2 within $\sim 10\%$. Hence, for $J = 2$ and 3, we admit a σ_r variation of $|\eta_r| < 0.1$. Assuming the same relative effect of this variation on the Einstein coefficients, we estimate a systematic uncertainty of $\pm 3\%$ for A_2 and A_3 , which is of similar order of magnitude as their statistical ones.

Differential laser depletion. Additional decays are expected in the normalized signals if photodetachment differently depletes the J -levels. An extreme upper limit for such effects is given by the observed decay constant $k_0 = 1.647(5) \times 10^{-3} \text{ s}^{-1}$ of the reference signal $N(\tilde{\nu}_r, t)$. Considering the variation of σ_r and the effect of the probing pulses at the various wave numbers, we estimate the differential laser depletion between $J = 1$ and $J = 0$ to represent $< 0.03k_0 \sim 5 \times 10^{-5} \text{ s}^{-1}$, which introduces a relative uncertainty of $\sim 1\%$ for A_1 . A wider limit of $< 0.1k_0 \sim 2 \times 10^{-4} \text{ s}^{-1}$ applies to $J \geq 2$, which again is of similar order of magnitude as the statistical uncertainties for these values.

Overall uncertainties. With $\sim 1\%$ uncertainties for both the J -dependence of σ_r and the differential laser depletion and a 1σ relative statistical uncertainty of 1.4%, we estimate the overall relative uncertainty of A_1 to 3.5%. For A_2 and A_3 the 1σ relative statistical uncertainties are 3.2% and 3.1%, respectively. Linearly adding the mentioned systematic uncertainty ranges, we estimate an overall relative uncertainty of 10% for A_2 and 7% for A_3 .

Electric deflection fields. The 60-keV OH^- beam is deflected by electric fields F up to 120 kV/m in the main CSR dipoles. This mixes a rotational state $|JM\rangle$ with neighboring levels $|J \pm 1 M\rangle$ where the admixture amplitude is, from the coupling matrix element [10],

$$|\varepsilon_{J',J}^M| = \frac{\mu F}{|E_J - E_{J'}|} \frac{\sqrt{J_{>}^2 - M^2}}{\sqrt{(2J_{>} + 1)(2J_{>} - 1)}} \leq |\varepsilon_{J',J}^0| \approx \frac{\mu F}{2|E_J - E_{J'}|} \quad (\text{S15})$$

with $J_{>} = \max(J, J')$. With $|E_J - E_{J'}| \geq 2B$ ($B = 2.32 \times 10^{-3} \text{ eV}$) and $\mu \sim 1 \text{ D}$, the interaction energy is $\mu F \sim 2.5 \times 10^{-6} \text{ eV}$ and the admixture amplitude $|\varepsilon_{J',J}^M| \lesssim 3 \times 10^{-4}$. Squared matrix elements for additional decay channels opening up by this admixture will be smaller than those of allowed decay channels by a factor of $|\varepsilon_{J',J}^M|^2 \lesssim 1 \times 10^{-7}$, which can be neglected. The steady-state

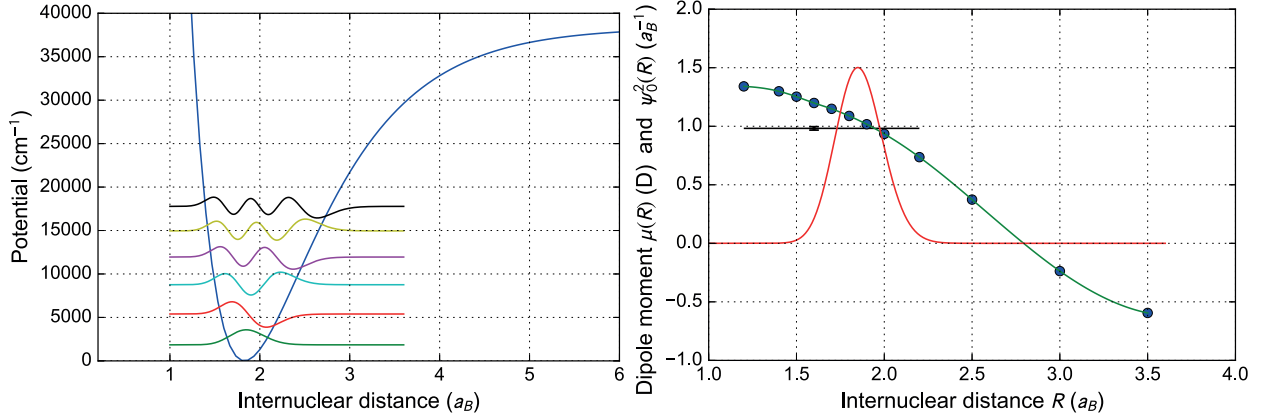


FIG. S3. Left: Morse potential of OH^- (parameters according to Ref. [8], p. 212, using $D_e = 38383.3 \text{ cm}^{-1}$, $\omega_e = 3731.0 \text{ cm}^{-1}$, and $r_e = 1.829 a_B$) and $v = 0$ to 5 vibrational wave functions (zero lines at the vibrational energies). Right: Dipole moment function $\mu(R)$ with values (dots) by Werner *et al.* [11], converted to the OH center-of-mass from Table V (MCFCF-SCEP) and cubic interpolation (line). Also shown is the $v = 0$ probability distribution of the internuclear distance R and the measured dipole moment from the main paper (horizontal line and overall uncertainty).

admixed populations $|\varepsilon_{J',J}^M|^2$ from different J levels are also much smaller than the typical relevant J -level populations occurring in the present experiment.

OH⁻ dipole moment function and vibrational averaging

In the relaxation and probing model, the Einstein A coefficients from Eq. (S12) can either be fixed by giving the molecular dipole moment μ_0 of OH^- or determined from the observed signal decays, as demonstrated in the main paper. In the latter case, each A_J offers the option of extracting an effective molecular dipole moment $\mu_{0,J}$ (see Table I of the main paper). Considering the discussion of the ro-vibrational line strength $S_{J',J''}$ in Bernath [8], p. 275f., using the Hönl-London factors and keeping the Herman-Wallis factor $F(m)$ [8] at 1 in the expression for $S_{J',J''}$ [Eq. (7.229)], the value μ_0 discussed in the main paper is equal to the vibrationally averaged dipole moment M_{00} , obtained with the vibrational wave functions for the $J = 0$ molecule. We have modeled the OH^- vibrational wave function using a Morse potential and calculated the average of the calculated dipole moment function $\mu(R)$ [11] (see Fig. S3), which yields $\mu_0 = M_{00} = 1.037 \text{ D}$. This is lower than the value at the equilibrium internuclear distance (Ref. [11], Table IV, MCFCF(5)-SCEP) by 0.035 and still deviates by 0.055 D or $\sim 5.3\%$ from the measured value, $\mu_0 = (0.982 \pm 0.015) \text{ D}$. Using the calculated μ_0 , the rotational lifetimes are underestimated with respect to the measured values by $\sim 10\%$. Calculating the wave function for $J = 1$ including

the centrifugal potential yields an estimated relative reduction of μ_0 by the Herman–Wallis factor (assuming the same electronic potential for all J) of only $\sim 2 \times 10^{-4}$ for the $1 \rightarrow 0$ transition.

Radiation field at the lowest OH^- transition

In the experiment, we derive $T_r = 15.1(1)$ K by sampling the radiation field on the transition $\tilde{\nu}_{J=0} = 37.47 \text{ cm}^{-1}$. The corresponding photon occupation number, from Eq. (S10), is $n(\tilde{\nu}_{J=0}) = 2.91(9) \times 10^{-2} = \bar{n}$. A plausible assumption is that the effective photon occupation number \bar{n} seen by the stored OH^- ions reflects a linear superposition of effects from the CSR vacuum chambers at a temperature near 6 K [12] and from openings towards room-temperature surfaces (300 K). With a fractional room-temperature influence of ϵ , the effective photon occupation number from this superposition would be $\bar{n} = \epsilon n_{300} + (1 - \epsilon)n_6$. Table SII lists photon occupation numbers for the radiative temperatures of 6 K (close to the measured temperature of the CSR vacuum chambers) and for a 300 K environment. With these values, we find $\epsilon \sim \bar{n}/n_{300} = 5.7(2) \times 10^{-3}$ for the fractional room-temperature influence. While it is difficult to estimate this value from the geometry, effective solid angles, reflection conditions, etc., this value is of the order of magnitude of the surface area that may be affected by room-temperature openings in the present arrangement of the CSR. In fact, a fraction of ϵ of the CSR circumference (35 m) amounts to ~ 20 cm, of the order of the beam tube diameter.

Contamination by $^{17}\text{O}^-$

In the data of Fig. 2 of the main paper, we find a background corresponding to a fraction of $(0.46 \dots 1.92) \times 10^{-2}$ of the rate at the reference $\tilde{\nu}_r$. Dividing by the laser-intensity normalization factor $S_0 \sim 3$ (see the main paper), this yields for the photodetachment background a fractional size of $(0.13 \dots 0.45) \times 10^{-2}$ compared to the reference photodetachment rate. We assume this reference rate to be dominated by OH^- . If we explain the background through a contamination by $^{17}\text{O}^-$,

TABLE SII. Photon occupation numbers for $\tilde{\nu}_{J=0} = 37.47 \text{ cm}^{-1}$ and various radiation field temperatures T_r .

Temperature (K)	$n(\tilde{\nu}_{J=0})$	Symbol
6	1.252×10^{-4}	n_6
15.1(1)	$2.91(9) \times 10^{-2}$	\bar{n}
300	5.079	n_{300}

the different photodetachment cross sections of OH^- and O^- must be considered. Taking Ref. [9] and the work cited therein, the O^- photodetachment cross section around 1.95 eV ($\sim 15\,751\text{ cm}^{-1}$) is smaller than that of OH^- at the same energy by a factor of ~ 0.75 , which yields a fractional abundance of $^{17}\text{O}^-$ in the stored beam of $(1.7 \dots 5.9) \times 10^{-3}$. This value is plausible considering the ratio of the $^{16}\text{O}^-$ and $^{16}\text{OH}^-$ peaks found in mass spectra of the applied sputter ion source and the $^{17}\text{O}^-$ natural abundance of 3.8×10^{-4} [13]. Variations of the value between runs can originate from changes of the ion source parameters. Moreover, the contaminating $^{17}\text{O}^-$ may be partially suppressed by the dispersion of the mass selecting magnet in the injection beamline of the CSR and the amount of the suppression can vary with the precise tuning of the injection beam line.

Photodetachment cross-section ratios for rotational population probing

For reference we give the probing wave numbers $\tilde{\nu}_k$ and the experimental photodetachment cross-section ratios for OH^- from this work, together with the model results (Table SIII). The measured ratios are precise enough (~ 3 to 16%) to serve as experimentally derived probing sensitivities and may be used to derive rotational population fractions from comparing photodetachment rates at specific probing wave numbers $\tilde{\nu}_k$.

TABLE SIII. Cross section ratios $\sigma_J(\tilde{\nu}_k)/\sigma_{J=0}(\tilde{\nu}_3)$ at the probing wave numbers $\tilde{\nu}_k$ using the results plotted in Fig. 3 of the main paper ($J = 0$ to 3). Measured results are compared to the model results where available. From the model, $\sigma_{J=0}(\tilde{\nu}_3)/\sigma_r = 0.3488$.

k	$\tilde{\nu}_k$	$J = 0$		$J = 1$		$J = 2$		$J = 3$	
		Exp.	Model	Exp.	Model	Exp.	Model	Exp.	Model
1	14879	1.52(5)	1.82	1.17(4)	1.64	1.31(12)	1.71		1.68
2	14859	1.08(4)	1.31	1.16(4)	1.57	1.24(10)	1.63		1.40
3	14769		1.00 ^a	0.587(21)	0.635	0.651(29)	0.791	0.89(12)	0.874
4	14732		0	0.603(20)	0.541	0.626(26)	0.629	0.71(9)	0.728
5	14672		0		0	0.179(11)	0.152	0.281(24)	0.220
6	14616		0		0		0	0.170(27)	0.167
7	14561		0		0		0		0.0124
8	14495		0		0		0		0
9	14428		0		0		0		0
10	14360		0		0		0		0

^a Reference value.

-
- [1] P. A. Schulz, R. D. Mead, and W. C. Lineberger, *Phys. Rev. A* **27**, 2229 (1983).
- [2] J. D. Rudmin, L. P. Ratliff, J. N. Yukich, and D. J. Larson, *J. Phys. B: At. Mol. Opt. Phys.* **29**, L881 (1996).
- [3] F. Goldfarb, C. Drag, W. Chaibi, S. Kröger, C. Blondel, and C. Delsart, *J. Chem. Phys.* **122** (2005), 10.1063/1.1824904.
- [4] J. P. Maillard, J. Chauville, and A. W. Mantz, *J. Mol. Spectrosc.* **63**, 120 (1976).
- [5] P. A. Schulz, R. D. Mead, P. L. Jones, and W. C. Lineberger, *J. Chem. Phys.* **77**, 1153 (1982).
- [6] S. Gewurtz, H. Lew, and P. Flainek, *Can. J. Phys.* **53**, 1097 (1975).
- [7] F. Breyer, P. Frey, and H. Hotop, *Z. Phys. A* **300**, 7 (1981).
- [8] P. F. Bernath, *Spectra of Atoms and Molecules*, 2nd ed. (Oxford University Press, New York, 2005).
- [9] P. Hlavenka, R. Otto, S. Trippel, J. Mikosch, M. Weidemüller, and R. Wester, *J. Chem. Phys.* **130**, 061105 (2009).
- [10] Y.-P. Chang, F. Filsinger, B. G. Sartakov, and J. Küpper, *Comp. Phys. Commun.* **185**, 339 (2014).
- [11] H. Werner, P. Rosmus, and E. Reinsch, *J. Chem. Phys.* **79**, 905 (1983).
- [12] R. von Hahn, A. Becker, F. Berg, K. Blaum, C. Breitenfeldt, H. Fadil, F. Fellenberger, M. Froese, S. George, J. Göck, M. Grieser, F. Grussie, E. A. Guerin, O. Heber, P. Herwig, J. Kartheim, C. Krantz, H. Kreckel, M. Lange, F. Laux, S. Lohmann, S. Menk, C. Meyer, P. M. Mishra, O. Novotný, A. P. O'Connor, D. A. Orlov, M. L. Rappaport, R. Repnow, S. Saurabh, S. Schippers, C. D. Schröter, D. Schwalm, L. Schweikhard, T. Sieber, A. Shornikov, K. Spruck, S. Sunil Kumar, J. Ullrich, X. Urbain, S. Vogel, P. Wilhelm, A. Wolf, and D. Zajfman, *Rev. Sci. Instrum.* **87**, 063115 (2016).
- [13] G. L. Molnár and R. B. Firestone, in *Handbook of Nuclear Chemistry*, edited by A. Vértes, S. Nagy, Z. Klencsár, R. G. Lovas, and F. Rösch (Springer US, 2011) pp. 475–610.